Journal of Photochemistry and Photobiology A: Chemistry 224 (2011) 116–122

Contents lists available at SciVerse ScienceDirect

Journal of Photochemistry and Photobiology A: Chemistry

journal homepage: www.elsevier.com/locate/jphotochem

# New pyran dyes for dye-sensitized solar cells

Samuel G. Awuah[a], Jason Polreis[a], Joshi Prakash[b], Qiquan Qiao[b], Youngjae You[a,*]

[a] Department of Chemistry and Biochemistry, South Dakota State University, Brookings, SD 57007, USA
[b] Department of Electrical Engineering and Computer Sciences, South Dakota State University, Brookings, SD 57007, USA

ARTICLE INFO

*Article history:*
Received 14 January 2011
Received in revised form 9 August 2011
Accepted 14 September 2011
Available online 18 September 2011

*Keywords:*
Pyran
Dye-sensitized solar cells (DSSCs)
Photosensitizer

ABSTRACT

Although ruthenium-based dyes have been extensively used in dye-sensitized solar cells (DSSCs) as photosensitizers, they have several shortcomings such as high costs and potential environmental toxicities. This has stimulated the development of highly efficient organic dyes as photosensitizers. We report the synthesis and photophysical, electrochemical and theoretical properties of novel pyran-based organic dyes (D1, D2, and D3) as well as their applications in DSSCs for the first time. The designed dyes possess a cyanoacrylic acid group as an acceptor and arylamine group as a donor group in a D-π-A configuration. The introduction of varying donor groups resulted in correspondingly different photophysical and electrochemical properties. The DSSCs fabricated using dye D1 showed the highest photovoltaic performance: a maximum incident photon-to-current conversion efficiency (IPCE) of 42%, a short-circuit current density (*Jsc*) of 4.76 mA cm$^{-2}$, an open circuit voltage (*Voc*) of 0.68 V, and a fill factor (FF) of 0.67, corresponding to an overall conversion efficiency of 2.17% under 100 mW cm$^{-2}$ irradiation. The synthesized dyes with a pyran chromophore and arylamine donor groups showed potentials for applications in DSSCs.



## 1. Introduction

The quest for alternative energy to supplant fossil resources has attracted a lot of attention in recent years. Proposed renewable sources include biofuels, wind, geothermal and solar energy. Among these, solar energy stands out as most promising taking into account the economic prospects. It could be estimated that about $3 \times 10^{24}$ J per year of energy is transported to the earth from the sun; this could account for about 10,000 times more than the total worldwide demand for energy [1–3]. The estimate may justify Gratzel's claim that covering 0.1% of the earth's surface with solar cells with an efficiency of 10% would satisfy our present needs [4,5].

Dye-sensitized solar cells (DSSCs) have showed great potential as a low cost alternative to silicon-based inorganic cells. Significant development in design and efficiency has been made in this area [6]. DSSCs combine optical absorption and charge separation processes using photosensitizers and $TiO_2$ nanocrystalline semiconductor film [7]. DSSCs with ruthenium-dyes, such as *cis*-di-(thiocyanato)-bis-(2,2-bipyridyl-4,4-dicarboxylate) ruthenium (II) (N3), showed high efficiencies up to ~11% [8,9]. However, they have long term stability issues and are expensive to manufacture due to the use of rare metals. These limitations have paved a way for the use of metal-free organic dyes as photosensitizers for DSSCs due to their high molar extinction coefficients, tunable band gap and optical properties, low cost of manufacturing and relative friendliness to the environment [10]. A number of classes of metal-free organic photosensitizers have been explored for DSSCs [11] such as porphyrins [12], phthalocyanines, coumarines [13], cyanines [14], merocyanines [15], hemicyanines [16], rhodamines [17], and boddipy [18].

Pyran-containing fluorescent (PCF) dyes has been used for organic light emitting diode (OLED) applications [19,20], red dopants for OLED [21–23], dye lasers [24,25], sensors [26] and bulk-heterojunction solar cells [27]. PCF dyes have numerous advantages which include higher molar extinction coefficients, tunable absorption properties, relatively accurate simulation of theoretical photoelectrochemical properties, and flexible synthesis for structural modification. In this study, we report the use of pyran based dyes and their applications in DSSCs for the first time. The dyes were designed to have D (donor)-π-A (acceptor) (or 2D-π-A) configuration to enhance conjugation length and absorption coefficient [2]; with pyran as the base chromophore, arylamines were used as donor moieties and cyanoacrylic acid as the acceptor and anchoring group.

## 2. Experimental details

### 2.1. General procedures in synthesis and photophysical determinations

All chemicals and materials were purchased from Sigma–Aldrich and Fisher, and were used without further purification.

* Corresponding author. Tel.: +1 405 271 6593x47473.
*E-mail address:* youngjae-you@ouhsc.edu (Y. You).

1010-6030/$ – see front matter © 2011 Elsevier B.V. All rights reserved.
doi:10.1016/j.jphotochem.2011.09.014

The UV–vis absorption spectra were measured in dilute solutions of chloroform recorded on an Ocean Optics (CHEMUSB4-UV-Fiber) spectrophotometer. The $^1$H NMR spectra were measured in $CDCl_3$ and DMSO-$d_6$ using a Bruker AVANCE 400 (400 MHz) spectrometer. Cyclic voltammetry measurements of dyes in THF solution using tetrabutylammonium perchlorate (TBAP) as supporting electrolyte were recorded on a Gamry Instruments reference 600 potentiostat. The DSSC devices were tested using a solar simulator (a xenon lamp from Newport, Model 67005 with a AM 1.5 filter) with a light intensity of 100 mW/cm$^2$ measured using an NREL calibrated Si cell and an Agilent 4155C Source Generator. Incident photon-to-current efficiency (IPCE) measurements were carried out by illuminating monochromatic light on the cells from an Oriel Monochromator (74001).

### 2.2. Synthesis

#### 2.2.1. *Methyl-2-cyano-2-(2,6-dimethyl-4H-pyran-ylidene)acetate (**1a**)*

2,6-Dimethyl-gamma-pyrone (6.2 g, 50 mmol), methyl cyanoacetate (5.4 g, 50 mmol), and acetic anhydride (25 ml) were mixed together and refluxed under nitrogen with stirring for 6 h. This resulted in a brown sludge that was allowed to cool to room temperature to induce precipitation. The precipitate was collected by vacuum filtration and washed well with methanol until all brown color was removed. The remaining residue was collected and recrystallized in methanol twice to obtain a pale white solid **1a** (2.3 g, 44.8%). $^1$H NMR (400 MHz, $CDCl_3$) $\delta$ 2.32 (s, 6H), 3.79 (s, 3H), 6.62 (s, 1H) 7.92 (s, 1H).

#### 2.2.2. *Methyl 2-(2,6-bis(4-(dimethylamino)styryl)-4H-pyran-4-ylidene)-2-cyanoacetate (**2a**)*

**1a** (1 g, 4.93 mmol) was dissolved in a solution of piperidine (0.73 ml, 7.39 mmol) and anhydrous acetonitrile (25 ml) under dry nitrogen atmosphere. 4-Dimethylaminobenzaldehyde (1.62 g, 10.85 mmol) was first dissolved in anhydrous acetonitrile (20 ml) and then added dropwise to the reaction with stirring. Then, the reaction solution was refluxed with stirring for 24 h. The crude was purified by column chromatography with a composed mobile phase of 20% ethyl acetate and 80% hexane with 1% acetic acid to give a pure compound **2a** (0.43 g 42.6%). $^1$H NMR (400 MHz, $CDCl_3$) $\delta$ 2.99 (s, 12H), 3.72 (s, 3H), 6.50–6.70 (m, 7H), 7.32–7.40 (m, 6H), 7.93 (s, 1H). MS (ESI); Calcd for $[C_{29}H_{29}N_3O_3]^+$ $m/z$: 467.22 Found: $m/z$ 468.3 $[M+H]^+$.

#### 2.2.3. *Methyl 2-(2,6-bis(4-(diphenylamino)styryl)-4H-pyran-4-ylidene)-2-cyanoacetate (**2b**)*

**1a** (0.25 g, 1.23 mmol) was dissolved in a solution of piperidine (0.18 ml, 1.85 mmol) and anhydrous acetonitrile (6 ml) under dry nitrogen atmosphere. 4-Diphenylaminobenzaldehyde (0.74 g, 2.71 mmol) was dissolved in anhydrous acetonitrile (7.75 ml) and added dropwise to the reaction with stirring. Then, the reaction mixture was heated to reflux. After 24 h the reaction was cooled in an ice bath and the precipitate was collected by vacuum filtration. Residue was washed with methanol and collected as **2b** (0.18 g, 70%). $^1$H NMR (400 MHz, $CDCl_3$) $\delta$ 3.79 (s, 3H), 6.61 ($J$ = 8 Hz, d, 1H), 6.65 ($J$ = 8 Hz, d, 1H), 7.03–7.05 ($J$ = 8 Hz, d, 2H), 7.08–7.15 (m, 14H), 7.26–7.32 (m, 8H), 7.38–7.42 (m, 6H), 8.03 (s, 1H). MS (ESI); Calcd for $[(C_{49}H_{37}N_3O_3)]^+$: $m/z$ 715.283. Found: $m/z$ 716.2914 $[M+H]^+$.

#### 2.2.4. *2-tert-Butyl-6-methyl-4H-pyrone [28]*

Sodium hydride (0.5 g, 12.3 mmol) was dissolved in dimethoxyethane (8.3 ml) under nitrogen. After mixture was at reflux temperature, acetylacetone (0.48 g, 4.1 mmol) in dimethoxyethane (4.2 ml) was added dropwise. After 45 min, methyl pivalate (0.42 g, 4.1 mmol) in dimethoxyethane (4.2 ml) was added dropwise. The reaction was left for 6 h and then cooled in an ice bath. Diethyl ether (12.5 ml) and cold water (8.3 ml) were added. Ether layer was extracted with cold water and then with a 1% sodium hydroxide solution. Ice (8.3 g) was added to aqueous layer and 12 N aqueous HCl (1.3 ml) was added. The aqueous layer was then extracted with 3 portions of diethyl ether. Ether was removed and then dried over sodium sulfate. Yellow oil (0.56 g) was obtained, which was then slowly dissolved in cold concentrated sulfuric acid and stirred for 10 min. The reaction was poured into ice water and neutralized with sodium bicarbonate. The resulting slurry was extracted with 4 portions of ether. Removal of the ether left a brownish oil. The crude was recrystallized from ethanol to obtain pure 2-*tert*-butyl-6-methyl-4H-pyrone (0.26 g 55%). $^1$H NMR (400 MHz, $CDCl_3$) $\delta$ 1.24 (s, 9H), 2.24 (s, 3H), 6.05 (s, 1H), 6.14 (s, 1H).

#### 2.2.5. *(2E)-Methyl 2-(2-tert-butyl-6-methyl-4H-pyran-4-ylidene)-2-cyanoacetate (1b)*

2-*tert*-Butyl-6-methyl-4*H*-pyrone (1.6 g, 9.6 mmol) and methyl cyanoacetate (0.95 g, 9.6 mmol), acetic anhydride (4.5 ml) were mixed together and refluxed under nitrogen with stirring for 6 h. This resulted in a brown sludge that was allowed to cool to room temperature to induce precipitation. The precipitate was collected by vacuum filtration and washed with methanol until all brown color was removed. The remaining residue was collected and recrystallized in methanol to obtain **1b** (0.43 g, 26.7%). $^1$H NMR (400 MHz, $CDCl_3$) $\delta$ 1.29 (s, 9H), 2.34 (s, 3H), 3.79 (s, 3H), 6.62 (s, 1H), 8.06 (s, 1H). MS (ESI); Calcd for $[C_{14}H_{17}NO_3]^+$: $m/z$ 247.1208. Found: $m/z$ 248.1280 $[M+H]^+$.

#### 2.2.6. *(2Z)-Methyl 2-(2-(4-(dimethylamino)styryl)-6-tert-butyl-4H-pyran-4-ylidene)-2-cyanoacetate (**2c**)*

**1b** (0.25 g, 1.01 mmol) was dissolved in a solution of piperidine (0.1 ml, 1.01 mmol) and anhydrous acetonitrile (6 ml) under dry nitrogen atmosphere. 4-Dimethylaminobenzaldehyde (0.18 g, 1.22 mmol) was dissolved in anhydrous acetonitrile (5 ml) and added dropwise to the reaction with stirring. After addition of 4-dimethylaminobenzaldehyde heated to reflux and left with stirring for 24 h. The reaction was then cooled to room temperature. Precipitate was collected by vacuum filtration and washed well with methanol. The residue was then recrystallized from methanol to obtain **2c** (0.17 g, 57.6%). $^1$H NMR (400 MHz, $CDCl_3$) $\delta$ 1.31 (s, 9H), 2.98 (s, 6H), 3.72 (s, 3H), 6.46 ($J$ = 16 Hz, 1H), 6.62 (s, 2H), 6.64 (s, 1H), 7.24 ($J$ = 16 Hz, 1H), 7.35 ($J$ = 8.4, d, 2H), 7.95 (s, 1H). MS (ESI); Calcd for $[C_{23}H_{26}N_2O_3]^+$: $m/z$ 378.194. Found: $m/z$ 379.2025 $[M+H]^+$.

#### 2.2.7. *(2E)-2-(2-(4-(Dimethylamino)styryl)-6-tert-butyl-4H-pyran-4-ylidene)-2-cyanoacetic acid (D1)[29]*

**2c** (0.15 g, 0.4 mmol) was dissolved in a mixture of tetrahydrofuran (15 ml) and 0.37 M LiOH in equal portions of water:ethanol (8 ml) then heated to 50 °C for 5 h. After evaporating the organic solvents the aqueous medium was acidified with ammonium chloride and extracted with ethyl acetate. The solid residue after evaporation was then recrystallized from ethanol to leave a red solid D1 (0.10 g, 69.3%). $^1$H NMR (400 MHz, DMSO-$d_6$) $\delta$ 1.32 (s, 9H), 2.99 (s, 6H), 6.55 (s, 1H), 6.62 ($J$ = 8 Hz, d, 2H), 6.92 ($J$ = 16 Hz, d, 1H), 7.34–7.24 ($J$ = 16 Hz, d, 1H), 7.46 ($J$ = 8 Hz, d, 2H), 7.80 (s, 1H), 12.18 (s, 1H). $^{13}$C NMR (DMSO): 171.1, 166.6, 160.4, 154.3, 151.9, 137.2, 130.0, 122.9, 119.6, 114.3, 112.3, 107.1, 101.8, 79.2, 36.7, 28.1. HRMS (ESI); Calcd for $[C_{22}H_{24}N_2O_3]^+$: $m/z$ 364.1787. Found: $m/z$ 365.1866 $[M+H]^+$.

#### 2.2.8. *2-(2,6-Bis(4-(dimethylamino)styryl)-4H-pyran-4-ylidene)-2-cyanoacetic acid (D2)*

Following the method in D1 and purification by silica gel column chromatography using 10% ethanol–methylene chloride, **2b**

(0.15 g, 0.32 mmol) was used to give D2 (0.08 g, 52.1%). $^1$H NMR (400 MHz, DMSO-$d_6$) $\delta$ 2.63 (s, 12H), 6.77 (s, 1H), 6.88 (s, 4H), 7.07 ($J$ = 15.9 Hz, d, 1H), 7.17 ($J$ = 15.9 Hz, d, 1H), 7.69–7.81 (m, 6H), 8.03 (s, 1H), 12.39 (s, 1H). $^{13}$C NMR (DMSO): 166.8, 159.6, 159.0, 153.5, 151.8, 137.7, 130.2, 123.2, 119.9, 114.6, 112.3, 107.4, 106.2, 78.4. HRMS (ESI); Calcd. for $[C_{28}H_{27}N_3O_3]^+$: $m/z$ 453.2052. Found: $m/z$ 454.2123 $[M+H]^+$.

#### 2.2.9. 2-(2,6-Bis(4-(diphenylamino)styryl)-4H-pyran-4-ylidene)-2-cyanoacetic acid (D3)

Following the method in D1, **2c** (0.2 g, 0.28 mmol) was used to give D3 (0.14 g, 72%). $^1$H NMR (400 MHz, DMSO-$d_6$) $\delta$ 6.58 (s, 1H), 6.76–6.79 (m, 1H), 6.94–7.06 (m, 15H), 7.19–7.23 (m, 8H), 7.44–7.58 (m, 7H), 7.83 (s, 1H) $^{13}$C NMR (DMSO): 166.5, 158.8, 158.2, 153.0, 149.2, 146.9, 136.5, 136.2, 130.2, 128.9, 125.5, 124.6, 121.6, 119.4, 118.0, 117.8, 108.6, 107.3, 80.4. HRMS (ESI); Calcd for $[C_{48}H_{35}N_3O_3]^+$: $m/z$ 701.2678. Found: $m/z$ 702.3989 $[M+H]^+$.

### 2.3. General procedures for preparation and evaluation of solar cells

DSSCs were prepared using D1, D2, and D3 (Fig. 1) as sensitizers and nanocrystalline anatase $TiO_2$ as photoanode following our previous fabrication method with some modifications [12]. The fluorine-doped tin dioxide (FTO) glasses were used as substrates (Hartford Glass Co. TEC-8, sheet resistance of ~8 Ω/sq, FTO thickness of ~400 nm and entire glass thickness of 2.3 mm). The substrates were cleaned using detergent, de-ionized (DI) water, acetone and IPA in an ultrasonic bath for 10 min each, followed by oxygen plasma for 10 min. The photoanodes were prepared by doctor blading the nanoparticle $TiO_2$ paste (Ti-Nanoxide HT-Solaronix) onto the FTO-glass substrate, which was precoated with a thin layer of compact $TiO_2$. The photoanode was then sintered at 450 °C for 45 min followed by being treated with $TiCl_4$ and sintered again as above. The area of the photoanode was 0.16 cm$^2$. Afterwards, the photoanode was soaked in a 0.5 mM dye solution in THF (D1, D2, and D3) or in a mixed solvent of 1:1 volume ratio acetonitrile and *tert*-butyl alcohol (N719) at room temperature for 12 h. The counter electrode was prepared by sputtering Pt onto the FTO glass substrates. The complete cell was then sealed using parafilm and the electrolyte was a redox couple of $I^-/I_3^-$ comprising 0.60 M BMII, 0.03 M $I_2$, 0.10 M GuSCN, 0.5 M *tert*-butyl pyridine in a mixed solvent of acetonitrile and valeronitrile (85:15 volume ratio).

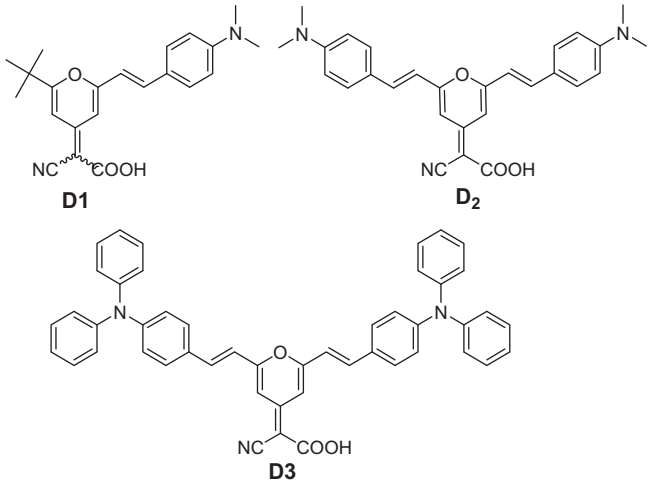


**Fig. 1.** Molecular structure of the pyran dyes.

## 3. Results and discussion

### 3.1. Design and synthesis of new photosensitizers

Three novel pyran-based dyes were designed to have "push–pull" configuration (D-π-A) for efficient electron injection to $TiO_2$ [30]. D2 and D3 were designed to see the effects of the numbers of D group and aromatic group at the D moiety. All of them were prepared following the flexible and straight forward synthetic route in only four steps (Scheme 1). Readily available respective arylamine aldehydes (donor groups) were adjoined to the pyran chromophore via the Knoevanegel condensation to give the highly conjugated pyrans **2a**–**c** in yields of 43–70%. These esters then were hydrolyzed under basic conditions to obtain the final products in good yields (52–72%).

### 3.2. Photophysical properties

The absorption spectra of all the compounds in dilute solutions of $CHCl_3$ were recorded at serial dilutions and the extinction coefficients were determined (Table 1). Normalized UV spectra were shown in Fig. 2. All the compounds exhibited good absorption properties: high extinction coefficient (48–92 × 10$^3$ M$^{-1}$ cm$^{-1}$) and wide absorption FWHM (full-width at half maximum) 104–113 nm. Since their absorption bands could be attributed to an intense delocalized aromatic π–π* transitions, the effects of the modifications in conjugated system on UV–vis spectra in solution were apparent. Increased number of D groups (D1 → D2) resulted in red-shift ($\lambda_{max}$, 446 → 459 nm) and higher extinction coefficient ($\lambda_{max}$, 48 → 79 × 10$^3$ M$^{-1}$ cm$^{-1}$). On the other hand, the impact of the number of aromatic groups at the D was minor (D2 → D3): absorption maxima ($\lambda_{max}$, 459 → 460 nm) and higher extinction coefficient ($\lambda_{max}$, 79 → 92 × 10$^3$ M$^{-1}$ cm$^{-1}$). Among the three dyes D3 showed the most preferable absorption properties as a sensitizer for DSSCs: wider absorption with higher extinction coefficient.

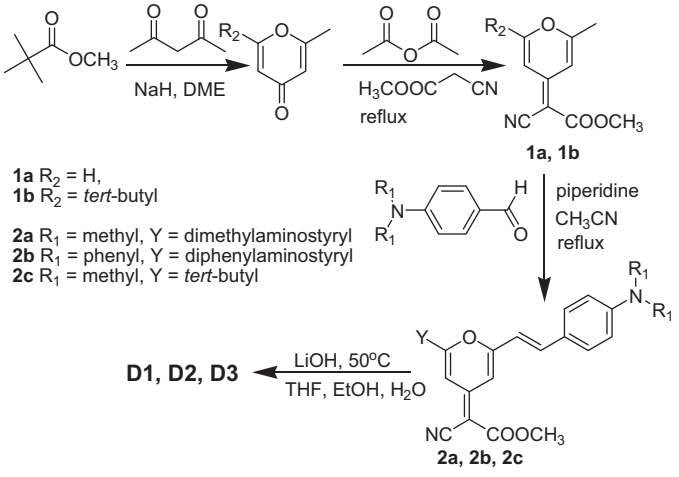


**Scheme 1.** Synthesis of the photosensitizers.

**Table 1**
Optical characteristics of sensitizers in solutions.

| Dye | $\lambda_{max}$[a](nm) [$\varepsilon$(×10$^3$ M$^{-1}$ cm$^{-1}$)] | $\lambda_{max}$[b](nm) | $\lambda_{em}$[c](nm) [Stokes shift (nm)] |
|---|---|---|---|
| D1 | 446 [48] | 411 | 570 [124] |
| D2 | 459 [79] | 422 | 623 [164] |
| D3 | 460 [92] | 382, 453 | 615 [155] |

[a] Maximum absorbance in $CHCl_3$.
[b] Maximum absorbance on $TiO_2$.
[c] Emission maxima of the dyes in $CHCl_3$.

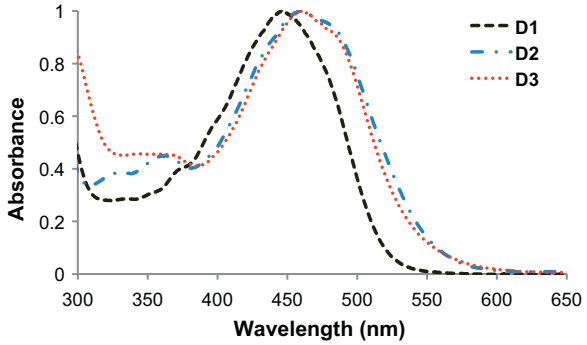


**Fig. 2.** Absorption spectra of pyran dyes in $CHCl_3$ ($1 \times 10^{-5}$ M).

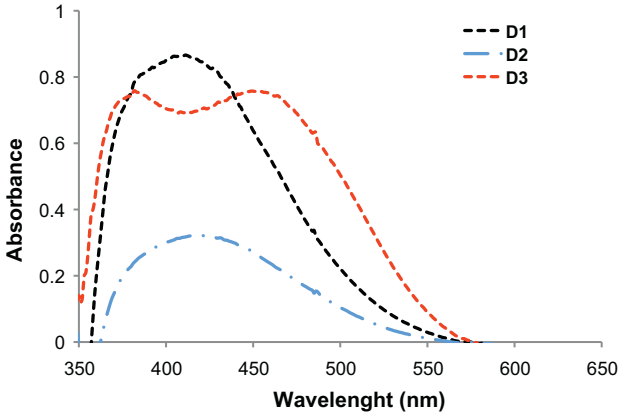


**Fig. 3.** Absorption spectra of pyran dyes on $TiO_2$ film.

All three dyes emitted bright fluorescence with relatively large Stokes shift (Table 1). The Stokes shift of D2 (164 nm) was larger than those of D1 (124 nm) possibly oweing to the two electronic donating groups. It was also slightly larger than that of D3 (155 nm).

The absorption spectra of all compounds on $TiO_2$ film were also made (Fig. 3 and Table 1). There were slight peak broadening and blue-shifting, presumably due to aggregation of the dyes on $TiO_2$ (Fig. 2 vs Fig. 3). The smaller absorbance of D2 on $TiO_2$ cells might be partially due to the lower dye attachment on $TiO_2$ than D1 and D3 (Fig. 3). However, there should be other factors for the lower absorbance of D2 film since the attached amount on $TiO_2$ of D2 was 78% of that of D3 while absorbance maximum of D2 was ~43% of that of D3 on $TiO_2$ film (Fig. 3 and Table 4). A noticeable observation was that the shape of absorbance spectrum of $TiO_2$ film with D3 was significantly different from that with D1. It showed two maxima at 383 and 453 nm and a broader spectrum, presumably due to higher and unique form of aggregation on $TiO_2$.

### 3.3. Electrochemical properties

Appropriate energy levels of highest occupied molecular obital (HOMO) and lowest unoccupied molecular obital (LUMO) of

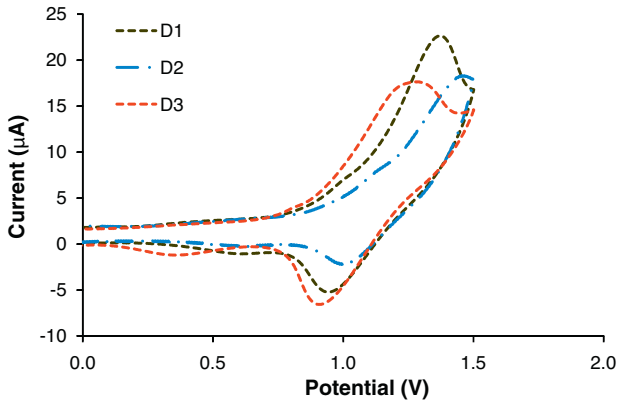


**Fig. 4.** Oxidative cyclic voltammetry of sensitizers measured in THF solution. The solution contained 0.1 M tetrabutylammonium perchlorate (TBAP) as a supporting electrolyte and $Ag/Ag^+$ as reference electrode and ferrocene as an internal standard.

sensitizers are important for effective electron injection to the conduction band of $TiO_2$ and electron acceptance from electrolytes ($I^-/I^{3-}$)[31,32]. Thus, these energy levels of the dyes were determined using cyclic voltammogram measurements (Fig. 4), which was recorded in a dry THF solution using tetrabutylammonium perchlorate (TBAP) as a supporting electrolyte and $Ag/Ag^+$ as reference electrode and ferrocene as the internal standard. Energy levels were calculated based on the standard method [33–35] (Table 2) using equation: $E_{HOMO/LUMO} = (-4.8 + E_{ref\ vs.\ Ag/Ag^+} - E_{OX/RED\ vs.\ Ag/Ag^+})$eV, where $E_{ref}$ is the potential of the ferrocene reference vs $Ag/Ag^+$ and $E_{OX/RED}$ is the onset potential for the oxidation or reduction vs $Ag/Ag^+$ of the pyran dyes. The estimated HOMO/LUMO energies is founded on the well known energy level of the ferrocene reference, 4.8 eV (below the vacuum level). For efficient dye regeneration the HOMO energy level should be sufficiently lower compared to the electrolyte redox potential. All the dyes D1, D2, and D3 displayed a reversible redox wave at a slightly high oxidation potential (HOMO: −5.49 eV to −5.56 eV), demonstrating possibility for electron transfer from the electrolyte. Furthermore, for efficient electron injection into the conduction band of $TiO_2$ the LUMO energy levels should be sufficiently higher compared to the $TiO_2$ conduction band edge [36]. In accessing the viability of the electron injection process from the excited dye molecule to $TiO_2$ conduction band we observed the LUMO energy levels of D1, D2, D3 (−3.64 to −3.69 eV) to be higher than the conduction band edge of $TiO_2$ (−4.24 eV).

### 3.4. Quantum chemistry and theoretical approach [37]

To gain insight into the electronic properties of these dyes, electron density maps of their frontier orbitals (HOMO and LUMO) were calculated using density functional theory (DFT), calculations in tandem with the Becke's three-parameter hybrid functional [38] and the Lee–Yang–Parr correlation [39] (B3LYP). Using Gaussian 09 [40] we applied a basis set of 6-311G* for our calculations. All the dyes showed similar electron density maps: in their ground state the electrons at HOMO are held in the donor moieties and

**Table 2**
HOMO and LUMO energy levels for D1, D2, and D3.

| Dye | HOMO[a] (eV) | LUMO[a] (eV) | HOMO[b] (eV) | LUMO[b] (eV) | HOMO[c] (eV) | LUMO[c] (eV) |
|---|---|---|---|---|---|---|
| D1 | −5.49 | −3.69 | −5.40 | −2.31 | −5.20 | −2.63 |
| D2 | −5.53 | −3.64 | −5.24 | −2.20 | −5.20 | −2.63 |
| D3 | −5.56 | −3.66 | −5.35 | −2.47 | −5.31 | −2.83 |

[a] HOMO and LUMO were obtained by comparison with the ionization potential of ferrocene and calculation from the oxidation potential respectively, scan rate, 100 mV/s.
[b] Calculated at the B3LYP/ 6-311G* in vacuo.
[c] Calculated at the B3LYP/6-311G* level in THF.

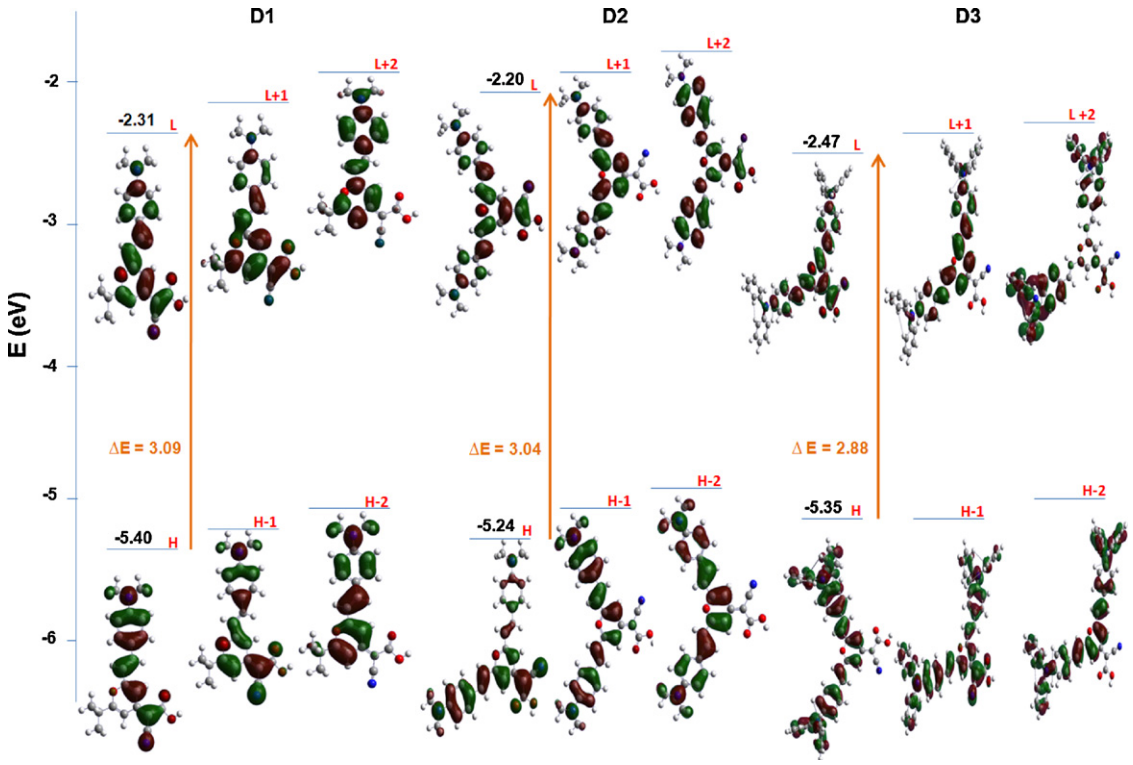


**Fig. 5.** Frontier orbitals of the sensitizers optimized with DFT at the B3LYP/6-311G* level. TDDFT calculations were performed using B3LYP/6-311G* level in vacuo and the C-PCM model in THF solution.

once excited (LUMO), the electrons move to the cyanoacrylic acid anchoring unit (Fig. 5). Such electron flows are expected to accelerate the electron injection from these pyran dyes to $TiO_2$.

To gain insight into the excited states as a result of the strong absorption bands in the visible region, we performed a TDDFT excited states calculations at the B3LYP/6-311G* level in vacuo and in solution (THF) using the C-PCM model, giving rise to a slight variation of ~50–60 nm between the two calculations. Considering the energy range, 2–3 transitions of sizable intensity ($f > 0.07$) were calculated and their respective excitation energies, oscillator strengths ($f$) and composition in terms of molecular orbital contributions are reported in Table 3. The lowest transition which is calculated at 2.89 eV, 2.70 eV and 2.50 eV of all the sensitizers (D1, D2 and D3 respectively) corresponds to a charge transfer (CT) excitation from the arylamine HOMO to the LUMO localized on the pyran-cyano acrylate moieties. In comparison with the experimental absorption maxima found at 2.78 eV, 2.70 eV, and 2.69 eV for D1, D2 and D3 respectively, the calculated transitions compared closely with the D1 calculated transition with a red-shifting (0.11 eV), D2 obtaining similar absorption maxima and D3 with a blue-shifting (0.19 eV). The good agreement between the experimental and the calculated transitions is indicative of the proper capturing of the charge-transfer character transition by the TDDFT calculation used. The transition calculated at 3.29 eV, 2.81 eV, 2.64 eV for D1, D2 and D3, is a $\pi$–$\pi^*$ excitation from HOMO-1 to the LUMO, taking place within the pyran-cyano acrylate moiety; while the less intense transition calculated at 3.82 eV for D1 is a $\pi$–$\pi^*$ excitation from HOMO to LUMO+1, corresponding to excitation within the arylamine moiety [41]. The red-shift of the calculated data by increased donor group (D1 → D2) was consistent with experimental data although the impact of the number of aromatic groups (D2 → D3) was not well predicted.

### 3.5. Current density–voltage characteristics

The IPCE and current density–voltage curves of the cells were determined (Figs. 6 and 7). DSSCs of D1 and D3 showed similar IPCE curves with a higher efficiency (42% for D1 cells) while DSSC of D2 seemed much less effective. The low IPCE efficiency and smaller *Jsc* of D2 cells were in agreement with the much smaller UV–vis

**Table 3**
Calculated TD-DFT and experimental excitation energies of low-lying transition for the sensitizers.

| Dye | State | Excitation[a] | $E$ (eV, nm) | $f^a$ | Excitation[b] | E[b] (eV, nm) | $f^b$ | Exp.[c](eV, nm) |
|---|---|---|---|---|---|---|---|---|
| D1 | $S_1$ | H → L (100%) | 2.89 (430) | 1.10 | H → L (99%) | 2.51 (493) | 1.39 | 2.78 (446) |
| | $S_2$ | H1 → L (80%) | 3.29 (377) | 0.08 | H1 → L (88%) | 3.36 (369) | 0.18 | |
| | $S_3$ | H → L1 (82%) | 3.82 (324) | 0.13 | H → L1(93%) | 3.56 (348) | 0.15 | |
| D2 | $S_1$ | H → L (83%) | 2.70 (458) | 0.96 | H → L (97%) | 2.29 (541) | 1.47 | 2.70 (459) |
| | $S_2$ | H1 → L (91%) | 2.81 (441) | 0.30 | H1 → L(98%) | 2.54 (487) | 0.72 | |
| D3 | $S_1$ | H → L (96%) | 2.50 (496) | 1.23 | H → L (95%) | 2.26 (549) | 1.48 | 2.69 (460) |
| | $S_2$ | H1 → L (94%) | 2.64 (469) | 0.34 | H1 → L (97%) | 2.44 (508) | 0.67 | |

H = HOMO, L = LUMO, H1 = next highest occupied molecular orbital (HOMO-1), H2 = HOMO-2, L1 = LUMO+1. In parenthesis is the composition in terms of molecular orbital contributions and $f$ is the oscillator strength calculated.

[a] Exctied state calculation at B3LYP/6-311G* in vacuo.
[b] Excited state calculation at B3LYP/6-311G* in THF.
[c] Experimental absorption maxima and excitation energies.

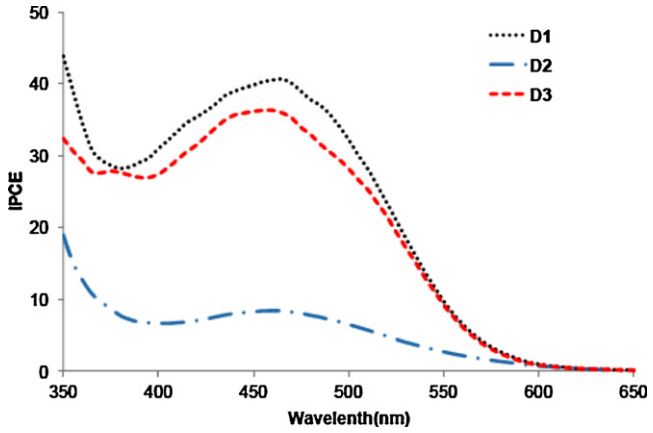


**Fig. 6.** IPCE curves of the pyran-based dye sensitized solar cells.

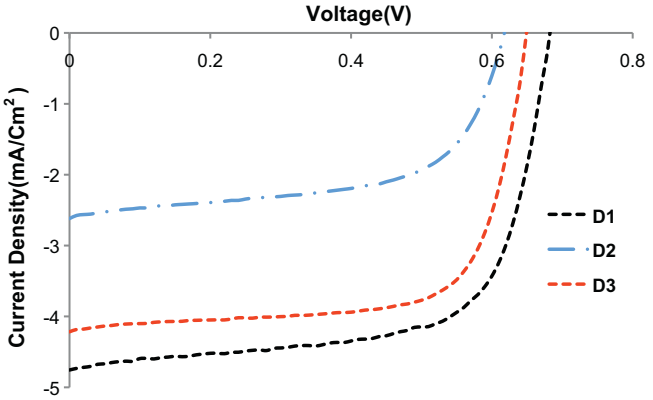


**Fig. 7.** Photocurrent density–voltage curves of dyes sensitized solar cells D1, D2, D3 under 100 mW/cm$^2$ simulated solar irradiation at AM 1.5.

**Table 4**
Device performance parameters of dye-sensitized solar cells.[a]

| Dye | *Jsc* (mA/cm$^2$) | *Voc* (V) | FF | $\eta$ (%) | Amount ($\times 10^{-5}$ mol/g)[b] |
|---|---|---|---|---|---|
| D1 | 4.76 | 0.68 | 0.67 | 2.17 | 1.3 |
| D2 | 2.61 | 0.61 | 0.61 | 1.00 | 0.7 |
| D3 | 4.21 | 0.64 | 0.73 | 1.92 | 0.9 |
| N719 | 13.16 | 0.85 | 0.63 | 7.05 | |

[a] Experiments were performed using $TiO_2$ photoelectrodes with 0.16 cm$^2$ working area on the FTO (8 Ω/sq) substrates.
[b] Amount of the dyes adsorbed per gram of $TiO_2$ film.

absorption spectrum for D2 sensitized $TiO_2$ film (Fig. 3). The smaller *Jsc* of D2 based cells might also be caused by both the lower dye attachment onto $TiO_2$ surface (Table 4) and other unknown factors. While the UV–vis spectrum of D3 on $TiO_2$ showed broader absorption than that of D1, DSSC of D3 did not show any better light harvesting efficiency than DSSC of D1. D3 might form aggregates on $TiO_2$ surface unfavorable for electron transfer.

The electron injection in these new designed dyes could occur from the arylamine donor moiety through the pyran chromophore to the conduction band of $TiO_2$. D1 based cells showed the highest efficiency due to its highest current density.

## 4. Conclusion

We synthesized three novel metal-free organic photosensitizers from the pyran family and, for the first time, fabricated $TiO_2$-based DSSCs using these pyran dyes. By using D-π-A (or 2D-π-A) configuration in the organic dye design, the DSSC device with D1 yielded a moderately high IPCE of 42% and a power conversion efficiency of ~2.17%. The donor moieties such as dimethylaminstyryl and diphenylaminestyryl enhanced the conjugation systems and thereby induced red-shifting (D1 < D2, D3) and increase of extinction coefficient (D1 < D2 < D3) of the pyran dyes in solution. Unfortunately, such favorable properties were not translated into the better light harvesting efficiency of DSSCs (D2 < D3 < D1), presumably due to the low dye attachement and other unknown factors on $TiO_2$ in cell fabrication process. However, this work clearly demonstrated great potential of using pyran-based dyes in DSSCs, which could be further optimized for improved energy conversion efficiency.

## Acknowledgements

This project is based upon work supported by the National Science Foundation (NSF)/EPSCoR Grant #EPS-0554609, NSF ECCS-0950731, and NASA EPSCoR grant #NNX09AP67A. Use of the Center for Nanoscale Materials was supported by the U.S. Department of Energy, Office of Science, Office of Basic Energy Sciences, under Contract No. DE-AC02-06CH11357. We are grateful to Dr. Brian Logue for his assistance in the electrochemical aspects, Drs. Brian Moore and Seth Darling for their helpful computational input and to Dr. Mahdi Farrokh Baroughi for his assistance in the *I–V* and IPCE measurement. A technical assist from Mr. Sudeep Karanjit is also appreciated.

## Appendix A. Supplementary data

Supplementary data associated with this article can be found, in the online version, at doi:10.1016/j.jphotochem.2011.09.014.

## References

[1] M. Gratzel, The artificial leaf, molecular photovoltaics achieve efficient generation of electricity from sunlight, Coordination Chemistry Reviews 111 (1991) 167–174.
[2] F.H. Chen, Z. Li, Organic D-pi-A dyes for dye-sensitized solar cell, Current Organic Chemistry (2007) 1241–1258.
[3] M. Gratzel, Perspectives for dye-sensitized nanocrystalline solar cells, Progress in Photovoltaics 8 (2000) 171–185.
[4] M. Gratzel, Photoelectrochemical cells, Nature 414 (2001) 338–344.
[5] A. Hagfeldt, M. Gratzel, Molecular photovoltaics, Accounts of Chemical Research 33 (2000) 269–277.
[6] L.M. Goncalves, V.D. Bermudez, H.A. Ribeiro, A.M. Mendes, Dye-sensitized solar cells: a safe bet for the future, Energy and Environmental Science 1 (2008) 655–667.
[7] B. Oregan, M. Gratzel, D. Fitzmaurice, Optical electrochemistry.2. Real-time spectroscopy of conduction-band electrons in a metal-oxide semiconductor electrode, Journal of Physical Chemistry 95 (1991) 10525–10528.
[8] M. Gratzel, Conversion of sunlight to electric power by nanocrystalline dye-sensitized solar cells (vol. 164, p. 3, 2004), Journal of Photochemistry and Photobiology A: Chemistry 168 (2004), 235–235.
[9] M.K. Nazeeruddin, M. Gratzel, Transition metal complexes for photovoltaic and light emitting applications, Photofunctional Transition Metals Complexes 123 (2007) 113–175.
[10] S. Ito, S.M. Zakeeruddin, R. Humphry-Baker, P. Liska, R. Charvet, P. Comte, M.K. Nazeeruddin, P. Pechy, M. Takata, H. Miura, S. Uchida, M. Gratzel, High-efficiency organic-dye-sensitized solar cells controlled by nanocrystalline-$TiO_2$ electrode thickness, Advanced Materials 18 (2006) 1202–1205.
[11] Z.N. Bing, X. Bai, Huaxue Jinzhan 20 (2008) 828–840.
[12] Y. Xie, P. Joshi, M. Ropp, D. Galipeau, L.F. Zhang, H. Fong, Y.J. You, Q.Q. Qiao, Structural effects of core-modified porphyrins in dye-sensitized solar cells, Journal of Porphyrins and Phthalocyanines 13 (2009) 903–909.
[13] K. Hara, Y. Tachibana, Y. Ohga, A. Shinpo, S. Suga, K. Sayama, H. Sugihara, H. Arakawa, Dye-sensitized nanocrystalline $TiO_2$ solar cells based on novel coumarin dyes, Solar Energy Materials and Solar Cells 77 (2003) 89–103.
[14] A. Ehret, L. Stuhl, M.T. Spitler, Spectral sensitization of $TiO_2$ nanocrystalline electrodes with aggregated cyanine dyes, Journal of Physical Chemistry B 105 (2001) 9960–9965.
[15] A.C. Khazraji, S. Hotchandani, S. Das, P.V. Kamat, Controlling dye (Merocyanine-540) aggregation on nanostructured $TiO_2$ films. An organized assembly approach for enhancing the efficiency of photosensitization, Journal of Physical Chemistry B 103 (1999) 4693–4700.

[16] Z.S. Wang, F.Y. Li, C.H. Huang, Photocurrent enhancement of hemicyanine dyes containing $RSO_3$-group through treating $TiO_2$ films with hydrochloric acid, Journal of Physical Chemistry B 105 (2001) 9210–9217.
[17] V.P.S. Perera, P.K.D.D.P. Pitigala, M.K.I. Senevirathne, K. Tennakone, A solar cell sensitized with three different dyes, Solar Energy Materials and Solar Cells 85 (2005) 91–98.
[18] S. Erten-Ela, M.D. Yilmaz, B. Icli, Y. Dede, S. Icli, E.U. Akkaya, A panchromatic boradiazaindacene (BODIPY) sensitizer for dye-sensitized solar cells, Organic Letters 10 (2008) 3299–3302.
[19] J.H. Kim, H. Lee, Synthesis, electrochemistry, and electroluminescence of novel red-emitting poly(p-phenylenevinylene) derivative with 2-pyran-4-ylidene-malononitrile obtained by the heck reaction, Chemistry of Materials 14 (2002) 2270–2275.
[20] Q. Peng, Z.Y. Lu, Y. Huang, M.G. Xie, S.H. Han, J.B. Peng, Y. Cao, Synthesis and characterization of new red-emitting polyfluorene derivatives containing electron-deficient 2-pyran-4-ylidene-malononitrile moieties, Macromolecules 37 (2004) 260–266.
[21] M.K. Leung, C.C. Chang, M.H. Wu, K.H. Chuang, J.H. Lee, S.J. Shieh, S.C. Lin, C.F. Chiu, 6-N,N-diphenylaminobenzofuran-derived pyran containing fluorescent dyes: a new class of high-brightness red-light-emitting dopants for OLED, Organic Letters 8 (2006) 2623–2626.
[22] C.S. Jianzhong, H.-J. Suh, S.-H. Kim, Synthesis and properties of conjugated copolymers with 2-pyran-4-ylidene malononitrile, Dyes and Pigments 68 (2006) 75–77.
[23] R.-H. Lee, L.-W. Liu, Electroluminescence and photovoltaic properties of light-emitting devices and solar cells comprising 2-pyran-4-ylidene-malononitrile conjugated polymers, Dyes and Pigments 84 (2010) 190–202.
[24] P. Frederiksen, T. Bjornholm, H.G. Madsen, K. Bechgaard, Electroluminescence of organic thin-films based on blends of polystyrene and fluorescent dyes, Journal of Materials Chemistry 4 (1994) 675–678.
[25] G. Kwak, C. Okada, M. Fujiki, H. Takeda, T. Nishida, T. Shiosaki, Polar laser dyes dispersed in polymer matrices: reverification of charge transfer character and new optical functions, Japanese Journal of Applied Physics 47 (2008) 1753–1756.
[26] Y.A. Son, S.Y. Gwon, S.Y. Lee, S.H. Kim, Synthesis and property of solvatochromic fluorophore based on D-pi-A molecular system: 2-{[3-Cyano-4-(N-ethyl-N-(2-hydroxyethyl)amino)styryl]-5,5-dimethylfuran-2(5H)-ylidene}malononitrile dye, Spectrochimica Acta Part A: Molecular and Biomolecular Spectroscopy 75 (2010) 225–229.
[27] J. L.H.Xue, X. Gu, Z. Yang, B. Xu, W. Tian, Efficient bulk-heterojunction solar cells based on a symmetrical D-π-A-π-D organic dye molecule, Journal of Physical Chemistry C 113 (2009) 12911–12917.
[28] Y.S. Yao, J. Xiao, X.S. Wang, Z.B. Deng, B.W. Zhang, Starburst DCM-type red-light-emitting materials for electroluminescence applications, Advanced Functional Materials 16 (2006) 709–718.
[29] Z.J. Ning, Q. Zhang, W.J. Wu, H.C. Pei, B. Liu, H. Tian, Starburst triarylamine based dyes for efficient dye-sensitized solar cells, Journal of Organic Chemistry 73 (2008) 3791–3797.
[30] T.M. Daniel, P. Hagberg, K.M. Karlsson, K. Nonomura, G.B. Peng Qin, T. Brinck, A. Hagfeldt, L. Sun, Tuning the HOMO and LUMO energy levels of organic chromophores for dye sensitized solar cells, Journal of Organic Chemistry (2007) 9550–9556.
[31] K. Hara, H. Arakawa, Dye-Sensitized Solar Cells, John Wiley & Sons, Ltd., 2005.
[32] A. Nattestad, A.J. Mozer, M.K.R. Fischer, Y.B. Cheng, A. Mishra, P. Bauerle, U. Bach, Highly efficient photocathodes for dye-sensitized tandem solar cells, Nature Materials 9 (2010) 31–35.
[33] J. Pommerehne, H. Vestweber, W. Guss, R.F. Mahrt, H. Bassler, M. Porsch, J. Daub, Efficient two layer leds on a polymer blend basis, Advanced Materials 7 (1995) 551–554.
[34] R. Zhu, G.A. Wen, J.C. Feng, R.F. Chen, L. Zhao, H.P. Yao, Q.L. Fan, W. Wei, B. Peng, W. Huang, Di-channel polyfluorene containing spiro-bridged oxadiazole branches, Macromolecular Rapid Communications 26 (2005) 1729–1735.
[35] R. Zhu, C.-Y. Jiang, B. Liu, S. Ramakrishna, Highly efficient nanoporous $TiO_2$-polythiophene hybrid solar cells based on interfacial modification using a metal-free organic dye, Advanced Materials 21 (2009) 994–1000.
[36] K. Hara, H. Arakawa, Dye-sensitized solar cells, in: A. Luque, S. Hegedus (Eds.), Handbook of Photovoltaic Science and Engineering, John Wiley & Sons, Ltd., 2003, pp. 663–700.
[37] C. Johnson, S. Darling, Y. You, Density functional theory as a guide for the design of pyran dyes for dye-sensitized solar cells, Monatshefte für Chemie/Chemical Monthly (2010) 1–8.
[38] A.D. Becke, Density-functional thermochemistry. 3. The role of exact exchange, Journal of Chemical Physics 98 (1993) 5648–5652.
[39] C. Lee, W. Yang, R.G. Paar, Physical Review B: Condensed Matter and Materials Physics (1988) 785–789.
[40] M.J. Frisch, G.W. Trucks, H.B. Schlegel, G.E. Scuseria, M.A. Robb, J.R. Cheeseman, G. Scalmani, V. Barone, B. Mennucci, G.A. Petersson, H. Nakatsuji, M. Caricato, X. Li, H.P. Hratchian, A.F. Izmaylov, J. Bloino, G. Zheng, J.L. Sonnenberg, M. Hada, M. Ehara, K. Toyota, R. Fukuda, J. Hasegawa, M. Ishida, T. Nakajima, Y. Honda, O. Kitao, H. Nakai, T. Vreven, J.A. Montgomery, Jr., J.E. Peralta, F. Ogliaro, M. Bearpark, J.J. Heyd, E. Brothers, K.N. Kudin, V.N. Staroverov, R. Kobayashi, J. Normand, K. Raghavachari, A. Rendell, J.C. Burant, S.S. Iyengar, J. Tomasi, M. Cossi, N. Rega, J.M. Millam, M. Klene, J.E. Knox, J.B. Cross, V. Bakken, C. Adamo, J. Jaramillo, R. Gomperts, R.E. Stratmann, O. Yazyev, A.J. Austin, R. Cammi, C. Pomelli, J.W. Ochterski, R.L. Martin, K. Morokuma, V.G. Zakrzewski, G.A. Voth, P. Salvador, J.J. Dannenberg, S. Dapprich, A.D. Daniels, Ö. Farkas, J.B. Foresman, J.V. Ortiz, J. Cioslowski, D.J. Fox, Gaussian, Inc., Wallingford CT, 2009.
[41] L.J.K. Kim S, S.O. Kang, J. Ko, J.-H. Yum, S. Fantacci, F. De Angelis, D. Di Censo, K. Nazeeruddin Md, M. Gratzel, Molecular engineering of organic sensitizers for solar cell applications, Journal of the American Chemical Society 128 (2006) 16701–16707.